Zinc-indiffused MgO:PPLN waveguides for blue/UV generation via VECSEL pumping

Research Article Vol. 59, No. 16 / 1 June 2020 / Applied Optics 4921

applied optics

Zinc-indiffused MgO:PPLN waveguides for blue/UV generation via VECSEL pumping

Alan C. Gray,[1,*] Jonathan R. C. Woods,[2] Lewis G. Carpenter,[1] Hermann Kahle,[3] Sam A. Berry,[1] Anne C. Tropper,[2] Mircea Guina,[3] Vasilis Apostolopoulos,[2] Peter G. R. Smith,[1] and Corin B. E. Gawith[1]

[1]Optoelectronics Research Centre, University of Southampton, University Road, Southampton, Hampshire SO17 1BJ, UK
[2]School of Physics and Astronomy, University of Southampton, University Road, Southampton, Hampshire SO17 1BJ, UK
[3]Optoelectronics Research Centre (ORC), Physics Unit Photonics, Faculty of Engineering and Natural Science, Tampere University, Korkeakoulunkatu 3,33720 Tampere, Finland
*Corresponding author: A.C.Gray@soton.ac.uk

Received 5 February 2020; revised 11 April 2020; accepted 15 April 2020; posted 16 April 2020 (Doc. ID 387839); published 27 May 2020

We present the design and characterization of a zinc-indiffused periodically poled lithium-niobate ridge waveguide for second-harmonic generation of ∼390 nm light from 780 nm. We use a newly developed, broadband near-infrared vertical external-cavity surface-emitting laser (VECSEL) to investigate the potential for lower-footprint nonlinear optical pump sources as an alternative to larger commercial laser systems. We demonstrate a VECSEL with an output power of 500 mW, containing an intracavity birefringent filter for spectral narrowing and wavelength selection. In this first demonstration of using a VECSEL to pump a nonlinear waveguide, we present the ability to generate 1 mW of ∼390 nm light with further potential for increased efficiency and size reduction.

https://doi.org/10.1364/AO.387839

1. INTRODUCTION

The generation of efficient and small-footprint UV sources for ion trapping is a topic of recent interest driven by a desire to create portable quantum systems for timing and navigation. Routes toward achieving low-footprint 369.5 nm sources are of particular interest for the Doppler cooling of Yb^+ ions [1]. It is preferable to use frequency-doubling in the process of generating this specific wavelength as near-IR lasers are commercially available and may be frequency-locked to molecular iodine at 739 nm [2]. It has been suggested in recent work by Mulholland *et al.* [3], during the development of a complete device for all Yb^+ ion trapping sources, that a 100 μW CW laser is the minimum requirement for this cooling application. Other lasers required for Yb^+ ion trapping include the photoionization, repumping, and state clear-out sources, but these wavelengths are typically longer with more readily available commercial sources.

The visible/near-IR pump source typically used for single-pass frequency-doubling to the blue/UV regime is a titanium sapphire laser [4–6], although the target wavelength can also be achieved via intracavity doubling with a Nd:YAG crystal and a suitable nonlinear media [7] or a ring cavity containing the nonlinear crystal where an external pump laser provides the infrared source [8,9]. While these lasers are ideal for laboratory use and initial characterization, their large footprint prohibits their use in volume critical applications.

For low size, weight, and power (SWAP) applications, periodically poled lithium-niobate (PPLN) remains a popular choice for frequency-doubling due to its tailorable quasi-phase-matched (QPM) structure and high d_{33} nonlinear coefficient [10]. PPLN waveguides are often favorable to bulk crystals due to the higher conversion efficiency attained from tighter confinement and overlap of the pump and generated signal mode compared with focused Gaussian beams [11]. Theoretically, conversion efficiency in waveguides scales quadratically with length in contrast with the linear scaling observed in bulk nonlinear crystals; this is the case for the focused condition shown to be optimal for efficient second-harmonic generation (SHG) in the low-conversion regime [12]. Short focal length optics also reduce the potential size of the nonlinear optical system. In this paper, we present zinc-indiffused PPLN diced ridge waveguides phasematched for ∼780 to 390 nm SHG as a route to achieve compact, low-power blue/UV wavelengths. Our large mode area approach [13] provides advantages in terms of coupling efficiency and power handling compared with recent lithium-niobate on insulator research, which has demonstrated high conversion efficiencies for low input powers [14]. We combine this with the first demonstration of a vertical external-cavity

surface-emitting laser (VECSEL) as the pump source for a $\chi^{(2)}$ nonlinear waveguide, investigating the goal of a potential small-footprint frequency-doubling solution.

We have chosen to investigate VECSELs as a single epitaxial growth yields hundreds of laser gain chips, making the technology extremely cost effective. A tailored active region design opens pathways to narrow linewidth operation [15–18], broadband sources for mode-locking [19–21], and wide tunability [22], while a tailored external cavity design allows for multiple wavelength generation [23,24] and variable pulse repetition rates [25]. Previous work incorporating nonlinear crystals into VECSELs has accomplished deep UV generation using second-harmonic generation with a single intracavity crystal [26] and third-harmonic generation with two birefringently phasematched, intracavity crystals [27]. Recently, high-power fundamental emission in the 780 nm region has been demonstrated at the watt level [28]. Vitally, VECSELs offer the ability to design shorter external cavities, such as that presented by Kuznetsov *et al.* [29]. This combination of wavelength tunability, output power, and potential for size reduction and beam quality in comparison with laser diodes provide an appropriate source for an investigation of blue/UV sources in combination with our nonlinear waveguides.

2. PPLN WAVEGUIDE FABRICATION

Our PPLN substrates are fabricated by applying a patterned photoresist to the $-z$ face of a 0.5 mm z-cut, 5% magnesium-doped $LiNbO_3$ (MgO:LN). An electric field greater than the material's coercive field is applied to the crystal via liquid electrodes to achieve domain reversal with a predefined period, Λ:

$$\Lambda = \frac{2\pi}{\Delta\beta}, \tag{1}$$

to satisfy phase-matching conditions where $\Delta\beta = \beta_{2\omega} - 2\beta_{\omega}$, representing the propagation constants of the associated SHG and fundamental modes. We investigated poling periods ranging from 2.2 to 2.4 μm to account for the discrepancy of the effective index of the zinc-indiffused waveguides from the Sellmeier equation and coefficients for bulk MgO:LN [30]. The resulting periodically poled domains traverse the entire 0.5 mm thickness of the crystal; due to the short period, the PPLN grating width was restricted to 200 μm to minimize local merging.

The waveguide fabrication process flow is illustrated schematically in Fig. 1. These fabrication steps are optimized via several iterative stages, starting with the deposition of a metallic zinc layer on unpoled LN followed by diffusion to form a planar waveguide. A study of the planar modal size is presented in Fig. 2(a) in which the modal size of a range of zinc-film thicknesses and indiffusion temperatures is displayed. The mode field diameter (MFD) was measured by imaging the waveguide output onto a calibrated InGaAs CCD camera. The measurement technique is further detailed in [31]. We proceeded with diffusion of a 150 nm thick metallic zinc layer at 900°C for 1 h in an oxygen environment, as this gives the smallest MFD and the highest probable overlap of pump and SHG guided modes. The waveguide was also single-mode in the y axis at ∼780 nm.

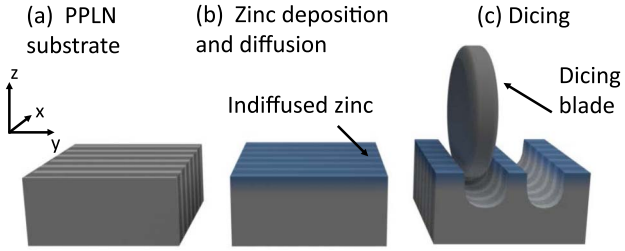

Fig. 1. Fabrication process flow of the zinc-indiffused PPLN waveguides.

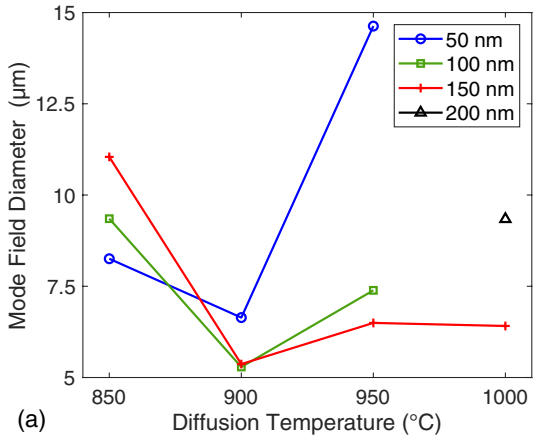

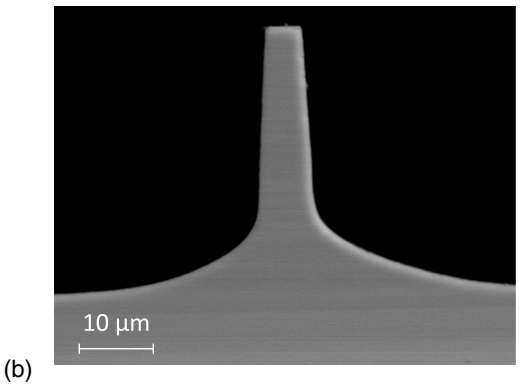

Fig. 2. (a) Mode field diameters of zinc-indiffusion planar layers versus metallic layer thickness and indiffusion temperature. (b) Example scanning electron micrograph in backscatter detection mode of a PPLN ridge waveguide.

Zinc deposition is carried out on a 50 mm × 10 mm PPLN chip. The ridge waveguide and end facets are formed via ultra-precision dicing. Waveguides widths were diced ranging from 5.7 to 8 μm, in each of the grating periods. The ∼780 nm mode was evidently multimodal in the x axis for widths above 7 μm. A scanning electron microscope image of one of these waveguides can be seen in Fig. 2(b). The blue/UV wavelength was multimodal in all fabricated waveguides. Further discussions on the waveguide platform, characterization methodologies, and its application in the 1560 to 780 nm frequency-doubling can be found in our recent work [31].

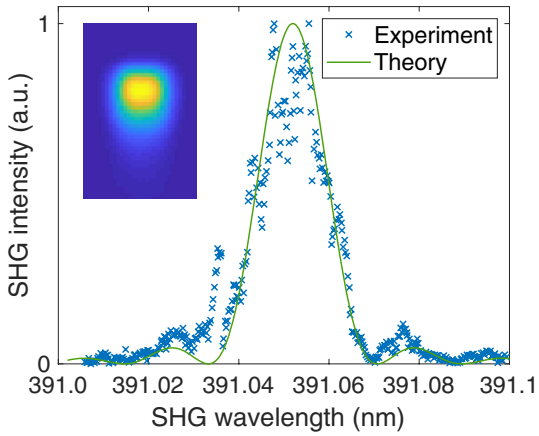

Fig. 3. PPLN waveguide phase-matching spectrum characterization performed through lock-in amplification detection at room temperature. Inset shows the output profile of the 780 nm mode propagating in this waveguide.

Initial characterization of the second-harmonic generation of the zinc-indiffused PPLN waveguides was carried out using a low-power, tuneable external cavity diode laser (ECDL) 780 nm laser (Sacher Lasertechnik). This source is fiber-coupled with polarization-maintaining fiber (PMF). The input coupling to the PPLN waveguide (PPLN:WG) was optimized via adjustable collimation and a focusing aspheric lens. The output was approximately collimated prior to prism separation of the pump and signal beams. The 390 nm beam was directed to a silicon photodiode and detected using lock-in amplification. The waveguides phasematched at a pump wavelength of ∼782.1 nm at room temperature with a 2.2 μm period grating, with the highest efficiency in a 5.7 μm wide ridge waveguide. The numerical aperture of the waveguide at the pump wavelength is approximately 0.11 with an MFD of 4.58 and 5.9 μm in the x and y axes, respectively. The resulting phase-matching spectrum for this waveguide is displayed in Fig. 3. The measurements with the ECDL 780 nm source provide a detailed phase-matching spectrum of the waveguide prior to the temperature-tuned phase-matching required for SHG in further experiments utilizing a VECSEL as the pump source; they also provide a coupling efficiency for comparison. While this phase-matching spectrum is close the theoretical curve, any deviations from the ideal $\mathrm{sinc}^2(\Delta\beta L/2)$ curve are known to result from fabrication nonuniformity [32,33]. The theoretical curve is calculated for a 14 mm waveguide, which is the length of the waveguide used in this work–indicating that the effective length must be fairly close to the actual physical length, which provides a general indicator of the poling quality and waveguide uniformity.

3. VECSEL CAVITY DESIGN AND CHARACTERIZATION

The VECSEL used in this work is a top emitter consisting of an active region similar to that described in [28]. The epitaxial surface of a single 4 × 4 mm gain chip sample was capillary bonded to a 350 μm × 5 × 5 mm silicon carbide (SiC) heat spreader using isopropyl alcohol. The two components were clamped to a copper heat sink with a 100 μm thick layer of

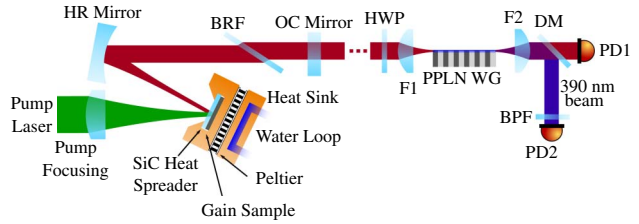

Fig. 4. VECSEL cavity configuration and the position of the PPLN waveguide in the setup, which is utilized as an extra-cavity component.

indium foil between the copper and the SiC as a thermal compound. The temperature of the copper heat sink was controlled with a PID servo and Peltier such that heat is exchanged into a water-cooled copper block. The entire assembly is mounted in a high-resolution micro-positioning mount.

The external cavity, shown schematically in Fig. 4, is formed from a 100 mm spherical concave high-reflecting fold mirror and a plane output coupler mirror with reflectivity of 97.5% at 780 nm. The gain sample to fold mirror distance is approximately 55 mm, and the fold mirror to output coupler distance is approximately 200 mm. In this external cavity configuration, the fundamental laser spatial mode has a radius of ∼48 μm $(1/e^2)$ at the gain sample's surface; further, with a cavity fold full angle of ∼24°, the fundamental mode radii at the plane OC mirror are 244 and 295 μm in the tangential and sagittal directions, respectively.

We use a Coherent Milennia EV laser as the VECSEL pump source and utilize up to 7 W of pump light at 532 nm. The pump light is incident on the gain sample at approximately 25° to the gain surface normal; further, approximately 22% of the pump light is spectrally reflected from the gain sample. The pump light is focused with a 75 mm achromatic lens, which is mounted on a linear translation stage to allow for pump spot size adjustment at the gain surface. The pump source emits a fundamental Gaussian spatial mode and, using the 75 mm lens, the pump beam waist was significantly smaller than the fundamental cavity spatial mode waist at the gain sample. Therefore, instead of using a longer focal length lens, the pump focusing lens is located specifically such that the pump light is brought to a waist in free space just before the gain sample, yielding a pump spot on the gain sample of radius ∼55 μm. Inside the laser cavity, a 4 mm thick quartz birefringent filter plate (BRF) is used to tune the emission wavelength. Spectral tuning of the VECSEL is achieved in steps of approximately 0.3 nm, due to the free spectral range of the etalon formed by the SiC heat spreader.

During operation, the gain structure's copper heat sink is maintained at 13.5°C. The VECSEL output power as a function of absorbed pump power, both with and without the intra-cavity BRF, is shown in Fig. 5(a). On insertion of the BRF into the laser cavity, the additional losses cause an increase in the threshold pump power. The spectral filtering effect of the BRF prevents the laser from operating on more than one SiC etalon fringe, and the resulting linewidth of the VECSEL remains narrow over the entire pump power and spectral tuning range. The VECSEL emission was monitored on an optical spectrum analyzer (Yokogawa AQ6370D) with 0.02 nm resolution; an example laser spectrum is shown in the inset in Fig. 5(a).

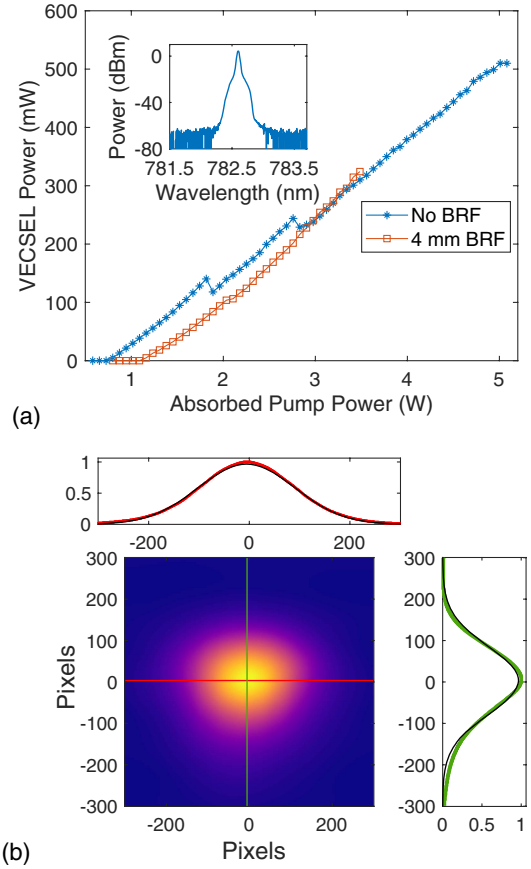

Fig. 5. (a) Power output of the VECSEL as a function of incident power, with and without the BRF, and spatial intensity profile of the laser emission. Here, we measure the power after all pump delivery optics and account for the calculated Fresnel reflection at the SiC-air surface. This inset displays an example optical spectrum of the laser in operation with the BRF included. Shoulders in the spectrum occur at approximately -20 dB of the spectral peak power. (b) Beam profile of the collimated output of the VECSEL.

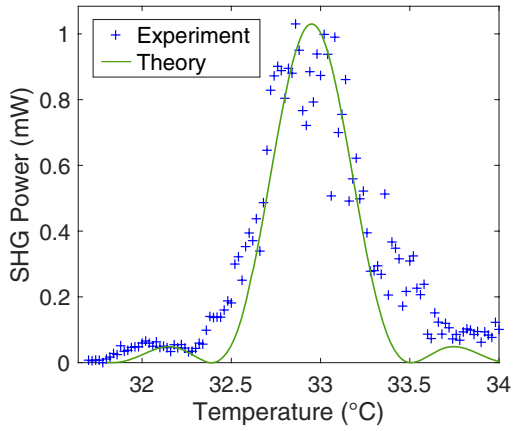

Fig. 6. Temperature sweep of the phase-matching spectrum pumped with the VECSEL.

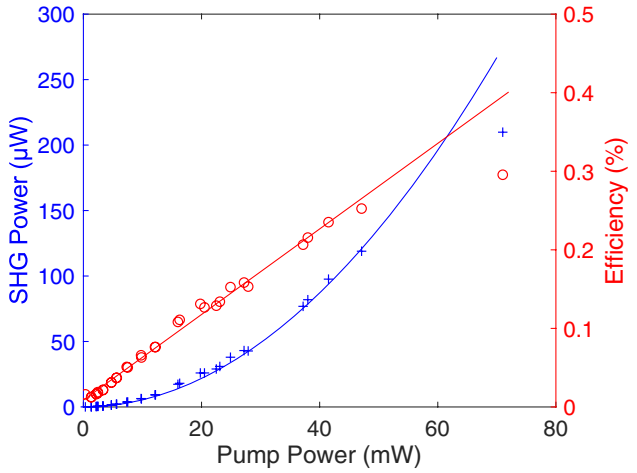

Fig. 7. SHG power as a function of pump throughput power for low pump powers. Taken via attenuation of the VECSEL beam directly after the output coupling mirror.

Efficient coupling to a single-mode waveguide forward of the laser cavity requires a good Gaussian beam profile. A beam profile of the VECSEL emission is given in Fig. 5(b), which represents the collimated beam approximately 75 cm from the output coupler.

4. BLUE/UV GENERATION

The PPLN is housed in a PV10 oven (Covesion Ltd.) capable of 0.01°C temperature stability and mounted to a five-axis translation stage. Insertion loss of the launched VECSEL beam is typically 4.7 dB using an 8 mm focal length aspherical lens (F1 in Fig. 4). This is in comparison with an insertion loss of 3 dB when using an optimized beam from a fiber-launched zoom collimator configuration, as shown schematically in our previous work [13]. This difference is due to a higher degree of alignment control and the ability to adjust the beam diameter when using an adjustable launch. Further investigation with input coupling focal length will be carried out in future work. As shown in Fig. 4, the output is collimated, and the spatially overlapped SHG signal and pump beams are separated using a dichroic mirror (DM) and monitored using silicon photodiodes. A further bandpass filter is implemented prior to the SHG photodiode, PD2, to ensure isolation of the correct signal. The loss of SHG power associated with the DM and BPF is 0.37 dB and is accounted for in the presented data.

At the operational wavelength of the VECSEL in use (782.86 nm), the PPLN was temperature-tuned to 33°C to achieve phase-matching, as demonstrated in Fig. 6. A maximum signal power of ∼1 mW was achieved with a pump throughput power of 120 mW, corresponding to an efficiency of 6.9 %/W, where efficiency is defined as $\eta = P_{2\omega}/P_{\omega}^2$. To further study the conversion efficiency, the power was controlled via a variable attenuator in the ∼780 nm beam path prior to the PPLN waveguide. The throughput power corresponds to the measured VECSEL power at PD1, as shown in Fig. 4. Analyzing the resulting data presented in Fig. 7 by linear regression fitting to the efficiency for pump powers up to 50 mW (low power/linear regime), we find an efficiency of $5.45 \pm 0.08\%/\mathrm{W}$.

The quadratic curve associated with the SHG power, $P_{2\omega}$, as presented in Fig. 7, is calculated as per the efficiency of this

device. Normalized to the nonlinear waveguide's relation to length, we obtain an efficiency of 2.78%/W · cm^2. While we note this is comparatively low to other blue-generating nonlinear waveguides [6], our frequency conversion utilized the first-order mode of the SH mode, reducing our nonlinear overlap integral [34]. Using the commercial waveguide modelling software FIMMWAVE (Photon Design Ltd.) as a numerical means for evaluating the overlap integral of the fundamental 780 nm mode with either the fundamental or first-order 390 nm modes, we would expect a twofold increase in the nonlinear overlap integral. Hence, a theoretical quadrupling of the conversion efficiency will be expected [11]; unfortunately, however, in this experiment and with the available poling periods, we were unable to access this regime.

In future work, we expect to target this phase-matching condition and improve our conversion efficiency. Further, investigating improvements into the grating structure for this fine-period grating, 2.2 μm, will also benefit this overall UV generation scheme. This is in addition to utilizing MgO:PPLN, which will allow wavelength generation further into the UV region than other second-order nonlinear waveguiding technologies; in addition, our zinc-indiffused platform will not be damage-threshold limited for the optical powers required for the relevant applications [13].

5. CONCLUSIONS

We present the first demonstration of SHG from a VECSEL gain structure in a $\chi^{(2)}$ nonlinear waveguide. Using a zinc-indiffused PPLN ridge waveguide with 2.2 μm poling period, we have achieved over 1 mW of UV/Blue SHG output power at 391.5 nm from the 783 nm VECSEL. While this initial result yielded a conversion efficiency of less than 6.9%/W, optimization of the VECSEL gain structure and further research into short-period poling of the lithium-niobate provide routes for improved efficiency of this UV laser source. Recent research presented by Kahle *et al.* [22] will be of use in further work in frequency-doubling a ∼739 nm laser source post-optimization of the gain structure toward the 369.5 nm required for Doppler cooling of Yb^+ ions.

Funding. Engineering and Physical Sciences Research Council (EP/M013294/1, EP/M024539/1, EP/T001046/1); Air Force Office of Scientific Research (FA9550-16-1-0531); Royal Academy of Engineering (RCSRF1718639).

Acknowledgment. We would like to thank Patrik Rajala and Sanna Ranta for growth of the VECSEL structure.

Disclosures. The authors declare no conflicts of interest.

REFERENCES

1. R. C. Sterling, H. Rattanasonti, S. Weidt, K. Lake, P. Srinivasan, S. Webster, M. Kraft, and W. K. Hensinger, "Fabrication and operation of a two-dimensional ion-trap lattice on a high-voltage microchip," Nat. Commun. **5**, 3637 (2014).
2. S. Olmschenk, K. C. Younge, D. L. Moehring, D. N. Matsukevich, P. Maunz, and C. Monroe, "Manipulation and detection of a trapped hyperfine qubit," Phys. Rev. A **76**, 052314 (2007).
3. S. Mulholland, H. Klein, G. Barwood, S. Donnellan, P. Nisbet-Jones, G. Huang, G. Walsh, P. Baird, and P. Gill, "Compact laser system for a laser-cooled ytterbium ion microwave frequency standard," Rev. Sci. Instru. **90**, 033105 (2019).
4. K. Mizuuchi, T. Sugita, K. Yamamoto, T. Kawaguchi, T. Yoshino, and M. Imaeda, "Efficient 340-nm light generation by a ridge-type waveguide in a first-order periodically poled MgO:$LiNbO_3$," Opt. Lett. **28**, 1344–1346 (2003).
5. A. C. Busacca, C. L. Sones, R. W. Eason, and S. Mailis, "First-order quasi-phase-matched blue light generation in surface-poled Ti: indiffused lithium niobate waveguides," Appl. Phys. Lett. **84**, 4430–4432 (2004).
6. C. Eigner, M. Santandrea, L. Padberg, M. F. Volk, C. E. Rüter, H. Herrmann, D. Kip, and C. Silberhorn, "Periodically poled ridge waveguides in KTP for second harmonic generation in the UV regime," Opt. Express **26**, 28827–28833 (2018).
7. M. Pierrou, F. Laurell, H. Karlsson, T. Kellner, C. Czeranowsky, and G. Huber, "Generation of 740 mW of blue light by intracavity frequency doubling with a first-order quasi-phase-matched crystal," Opt. Lett. **24**, 205–207 (1999).
8. R. Le Targat, J.-J. Zondy, and P. Lemonde, "75%-efficiency blue generation from an intracavity PPKTP frequency doubler," Opt. Commun. **247**, 471–481 (2005).
9. F. Villa, A. Chiummo, E. Giacobino, and A. Bramati, "High-efficiency blue-light generation with a ring cavity with periodically poled KTP," J. Opt. Soc. Am. B **24**, 576–580 (2007).
10. I. Shoji, T. Kondo, A. Kitamoto, M. Shirane, and R. Ito, "Absolute scale of second-order nonlinear-optical coefficients," J. Opt. Soc. Am. B **14**, 2268–2294 (1997).
11. W. P. Risk, T. Gosnell, and A. Nurmikko, *Compact Blue-Green Lasers* (Cambridge University, 2003).
12. G. Boyd and D. Kleinman, "Parametric interaction of focused gaussian light beams," J. Appl. Phys. **39**, 3597–3639 (1968).
13. S. A. Berry, L. G. Carpenter, A. C. Gray, P. G. R. Smith, and C. B. E. Gawith, "Zn-indiffused diced ridge waveguides in MgO:PPLN generating 1 watt 780 nm SHG at 70% efficiency," OSA Continuum **2**, 3456–3464 (2019).
14. L. Chang, Y. Li, N. Volet, L. Wang, J. Peters, and J. E. Bowers, "Thin film wavelength converters for photonic integrated circuits," Optica **3**, 531–535 (2016).
15. M. A. Holm, D. Burns, A. I. Ferguson, and M. D. Dawson, "Actively stabilized single-frequency vertical-external-cavity AlGaAs laser," IEEE Photon. Technol. Lett. **11**, 1551–1553 (1999).
16. D. Pabœuf and J. E. Hastie, "Tunable narrow linewidth AlGaInP semiconductor disk laser for Sr atom cooling applications," Appl. Opt. **55**, 4980–4984 (2016).
17. P. Moriya and J. Hastie, "Sub-kHz linewidth VECSEL for cold atom experiments," in *Laser Congress 2018 (ASSL)* (Optical Society of America, 2018), p. ATh5A.4.
18. Y. Kaneda, M. Hart, S. H. Warner, J.-P. Penttinen, and M. Guina, "Narrow-linewidth operation of folded 1178nm vecsel with twisted-mode cavity," Opt. Express **27**, 27267–27272 (2019).
19. S. Hoogland, S. Dhanjal, A. C. Tropper, J. S. Roberts, R. Haring, R. Paschotta, F. Morier-Genoud, and U. Keller, "Passively mode-locked diode-pumped surface-emitting semiconductor laser," IEEE Photon. Technol. Lett. **12**, 1135–1137 (2000).
20. U. Keller and A. C. Tropper, "Passively modelocked surface-emitting semiconductor lasers," Phys. Rep. **429**, 67–120 (2006).
21. C. R. Head, T. C. Sverre, J. Woods, A. Hein, M. Polanik, A. P. Turnbull, E. A. Shaw, P. Unger, A. C. Tropper, and V. Apostolopoulos, "Study of dielectric coatings for broadband operation of surface-emitting semiconductor lasers," J. Opt. Soc. Am. B **36**, 752–756 (2019).
22. H. Kahle, K. Nechay, J.-P. Penttinen, A. Tukiainen, S. Ranta, and M. Guina, "AlGaAs-based vertical-external-cavity surface-emitting laser exceeding 4 W of direct emission power in the 740–790 nm spectral range," Opt. Lett. **43**, 1578–1581 (2018).
23. R. Paquet, S. Blin, M. Myara, L. L. Gratiet, M. Sellahi, B. Chomet, G. Beaudoin, I. Sagnes, and A. Garnache, "Coherent continuous-wave dual-frequency high-Q external-cavity semiconductor laser for GHz–THz applications," Opt. Lett. **41**, 3751–3754 (2016).
24. J. Woods, D. Heath, J. Daykin, T. C. Sverre, B. Keenlyside, B. Mills, I. Sagnes, G. Beaudoin, S. Blin, A. Garnache, A. Tropper, and V.

Apostolopoulos, "Semiconductor disk laser in bi-frequency operation by laser ablation micromachining of a laser mirror," Opt. Express **27**, 22316–22326 (2019).
25. T. Chen Sverre, J. R. C. Woods, M. Polanik, P. Unger, A. C. Tropper, and V. Apostolopoulos, "Continuous repetition rate tuning from 960 MHz to 1.72 GHz of a sub-300 femtosecond mode-locked semiconductor disk laser," Appl. Phys. Lett. **113**, 161106 (2018).
26. J. E. Hastie, L. G. Morton, A. J. Kemp, M. D. Dawson, A. B. Krysa, and J. S. Roberts, "Tunable ultraviolet output from an intracavity frequency-doubled red vertical-external-cavity surface-emitting laser," Appl. Phys. Lett. **89**, 061114 (2006).
27. J. M. Rodrguez-Garca, D. Pabœuf, and J. E. Hastie, "Tunable, CW laser emission at 225 nm via intracavity frequency tripling in a semiconductor disk laser," IEEE J. Sel. Top. Quantum Electron. **23**, 1–8 (2017).
28. H. Kahle, J.-P. Penttinen, H.-M. Phung, P. Rajala, A. Tukiainen, S. Ranta, and M. Guina, "Comparison of single-side and double-side pumping of membrane external-cavity surface-emitting lasers," Opt. Lett. **44**, 1146–1149 (2019).
29. M. Kuznetsov, F. Hakimi, R. Sprague, and A. Mooradian, "High-power (>0.5-W CW) diode-pumped vertical-external-cavity surface-emitting semiconductor lasers with circular TEM_{00} beams," IEEE Photon. Technol. Lett. **9**, 1063–1065 (1997).
30. O. Gayer, Z. Sacks, E. Galun, and A. Arie, "Temperature and wavelength dependent refractive index equations for MGO-doped congruent and stoichiometric $LiNbO_3$," Appl. Phys. B **91**, 343–348 (2008).
31. L. G. Carpenter, S. A. Berry, R. H. S. Bannerman, A. C. Gray, and C. B. E. Gawith, "ZnO indiffused MgO:PPLN ridge waveguides," Opt. Express **27**, 24538–24544 (2019).
32. A. C. Gray, S. A. Berry, L. G. Carpenter, J. C. Gates, P. G. R. Smith, and C. B. E. Gawith, "Investigation of PPLN waveguide uniformity via second harmonic generation spectra," IEEE Photon. Technol. Lett. **32**, 63–66 (2020).
33. M. Santandrea, M. Stefszky, and C. Silberhorn, "General framework for the analysis of imperfections in nonlinear systems," Opt. Lett. **44**, 5398–5401 (2019).
34. R. Regener and W. Sohler, "Efficient second-harmonic generation in Ti:$LiNbO_3$ channel waveguide resonators," J. Opt. Soc. Am. B **5**, 267–277 (1988).